Chinese Journal of
POLYMER SCIENCE

RESEARCH ARTICLE

https://doi.org/10.1007/s10118-026-3753-z
Chinese J. Polym. Sci.

From Global to Localized Illumination: Tunable Photo-induced Patterns in a Ternary Reaction-diffusion System

Zhuo-Hang Cai[a], Chang-Hao Li[b,c*], and Jian-Feng Li[a*]

[a] *The State Key Laboratory of Molecular Engineering of Polymers, Department of Macromolecular Science, Fudan University, Shanghai 200433, China*
[b] *College of Energy Engineering and State Key Laboratory of Clean Energy Utilization, Zhejiang University, Hangzhou 310003, China*
[c] *Joint Research Centre on Medicine, Xiangshan Hospital of Wenzhou Medical University, Ningbo 315700, China*

Electronic Supplementary Information

Abstract Photo-induced reaction-diffusion systems provide a valuable theoretical framework for exploring nonequilibrium self-organization under external energy input. Most existing studies have focused on binary mixtures subjected to globally uniform driving, whereas realistic chemical and biological systems are typically multicomponent and experience strongly localized energy supply. In this work, we extend photo-induced reaction-diffusion models to a multicomponent setting and systematically investigate pattern formation in a minimal three-component system. By combining numerical simulations with linear stability analysis, we find illumination can induce periodic nonequilibrium structures, whose characteristic length scales can be tuned by the input energy density and intrinsic molecular energetic parameters. We further introduce localized illumination to capture the effects of spatially heterogeneous energy input. Under such conditions, a theoretical phase diagram for pattern formation is constructed, revealing distinct spatial morphologies, including dot patterns and target-like structures. In addition, we explicitly examine the nonnegativity of entropy production for both globally and locally illuminated systems. These results provide a unified and physically consistent framework for understanding photo-induced pattern formation in multicomponent nonequilibrium systems and are also applicable to photoexcitation-controlled supramolecular systems such as persulfurated-arene/block-copolymer assemblies.

Keywords Reaction-diffusion system; Nonequilibrium thermodynamics; Phase separation; Photo-reaction

Citation: Cai, Z. H.; Li, C. H.; Li, J. F. From global to localized illumination: tunable photo-induced patterns in a ternary reaction-diffusion system. *Chinese J. Polym. Sci.* https://doi.org/10.1007/s10118-026-3753-z

INTRODUCTION

The origin of life remains a central question in natural sciences. Living systems are generally believed to have emerged from early chemical processes on primitive Earth, where simple organic molecules have gradually evolved into increasingly complex assemblies through reaction networks and self-organization.[1] During both their emergence and subsequent evolution, living systems continuously exchange matter and energy with their surroundings, giving rise to highly ordered structures maintained under nonequilibrium conditions.[2] To investigate the nonequilibrium thermodynamics underlying such biological organization, a wide range of theoretical models have been developed with the aim of capturing the essential features of living systems while remaining as simple and general as possible.[3–5] Among these approaches, reaction-diffusion models constitute one of the most widely adopted theoretical frameworks.[6]

Over the past half-century, reaction-diffusion models have been successfully applied to a broad spectrum of biological phenomena, including spatial pattern formation in animal skin and plant organs,[7,8] cell polarization and chemotaxis,[9] phytoplankton-oxygen systems, inflammatory signal propagation,[10] and spatiotemporal population dynamics in ecological systems.[11] Early reaction-diffusion models often adopted idealized mixtures and neglected the intermolecular interactions. Over the last three decades, reaction-diffusion models have been systematically refined by incorporating interaction and chemical activity corrections.[12–14] Recently, a systematic classification of instabilities in non-ideal reaction-diffusion systems distinguishes diffusion-driven instabilities (E-type) leading to phase-separation-like behavior and reaction-driven instabilities (R-type) originating from oscillating chemical reactions,[15] which provides a rigorous foundation for the construction and stability analysis of multicomponent reaction-diffusion models. However, most previous discussions have focused on thermally induced reaction-diffusion models, while photo-induced chemical reactions may show different results, disobeying this R/E-type classification.

Photochemical reactions represent a ubiquitous class of nonequilibrium processes in nature; however, their role in reaction-diffusion systems has received comparatively limited

* Corresponding authors, E-mail: changhao.li@zju.edu.cn (C.H.L.)
E-mail: lijf@fudan.edu.cn (J.F.L.)
Received April 3, 2026; Accepted May 19, 2026; Published online July 24, 2026

attention. Some theoretical studies have demonstrated that photo-driven reactions can drive systems away from thermodynamic equilibrium in oscillating chemical reaction systems (R-type instability).[16,17] Our previous work focused on binary interconversion systems under continuous illumination. The emergence of stable dissipative structures has also been reported,[18] and the dependence of their characteristic length scales on the negative entropy flux, quantified by the incident light intensity, has been systematically analyzed. These results indicate that photochemical reactions provide a physically grounded and externally controllable driving mechanism for nonequilibrium structure formation, which is not due to the E-type instability in thermal reaction systems. However, realistic chemical and biological systems are inherently multicomponent, with reaction networks that are substantially more complex than those captured by binary models. This limitation becomes particularly evident in photoexcitation-controlled supramolecular systems, such as persulfurated-arene/block-copolymer assemblies, where irradiation continuously tunes the effective phase-volume ratio and enables access to a wide range of ordered structures.[19] In such contexts, binary descriptions are no longer sufficient to capture the essential physics.

Moreover, most reaction-diffusion models focus on homogeneous energy and material supply or supply through the boundary, whereas spatially localized input has been much less studied.[20,21] In biological systems, such as eukaryotic cells, most of the energy to be utilized is released from the localized organelle mitochondria.

In this work, photo-induced reaction-diffusion models are extended to multicomponent systems, and the mechanisms of pattern formation driven by photoisomerization reactions are systematically investigated. A minimal three-component system is employed as a representative model to establish a generalizable framework for higher-dimensional multicomponent systems and to provide physical insight into the emergence of biological order under nonequilibrium conditions. In addition, the concept of localized illumination is introduced to account for spatially heterogeneous energy input, enabling the exploration of structure formation in confined reactive regions and extending the relevance of reaction-diffusion models in the context of the origin of life.

LIGHT-INDUCED PATTERN FORMATION UNDER GLOBAL ILLUMINATION

Model Construction

In our previous work,[18] the reaction kinetics for photo-induced processes with a clear microscopic origin were systematically derived, and the resulting model was shown to accurately describe light-induced pattern formation in binary systems. To improve generality while retaining essential physical ingredients, theoretical models of biological organization are preferably formulated in a minimal manner. In this study, we consider a ternary mixture with a photo-excited intermediate composed of components A, B, C, and M. The system undergoes a reversible photo-induced interconversion reaction A ⇌ M ⇌ B with M as the transition state of photoreaction.[22] Component B is assumed to be fully miscible with both A and C, whereas phase separation occurs only between A and C, characterized by a nonzero interaction parameter χ_{AC}, whereas χ_{AB} and χ_{BC} vanish. This separation of structural and reactive roles is motivated by recent light-regulated supramolecular and polymer assembly experimental results,[19,23–25] which suggest that light often controls the morphology by changing the effective composition or transient activity of the system. Therefore, in our model, A and C are assigned the role of structural components that provide the dominant thermodynamic incompatibility, whereas B acts as a miscible photo-regulated species that redistributes composition through the reaction pathway. Retaining only χ_{AC} allows isolation of the coupling between structural phase separation and photo-driven conversion. Restricting the model to a single nonzero interaction parameter can be understood as a coarse-grained minimal and controllable description of the multicomponent behavior.

Within the Flory-Huggins framework, the free energy of the system can be written as

$$F = \rho_0 k_B T \int d\mathbf{r} \Big[\sum_{x\in\{A,B,C,M\}} (\phi_x \ln\phi_x + \phi_x \epsilon_x) + \chi \phi_A \phi_C + \frac{b_A}{2}|\nabla\phi_A|^2 + \frac{b_B}{2}|\nabla\phi_B|^2 + \frac{b_C}{2}|\nabla\phi_C|^2 \Big] \tag{1}$$

where ρ_0 is the averaged density of the system, k_B is the Boltzmann constant, T is the temperature, ϕ_x is the volume fraction of component x, ϵ_x is the molecular internal energy, and b_x is the gradient coefficient.

To evaluate the thermodynamic quantities associated with photoreaction process, the light intensity is parameterized using blackbody radiation. For relatively weak incident light with angular frequency ω, the intensity is as follows:[26]

$$I_{T_b,\Omega_b}(\omega) = \frac{\Omega_b}{4\pi} I_0(\omega) = \frac{\hbar\Omega_b}{4\pi^3 c^3} \frac{\omega^3}{e^{\hbar\omega/(k_B T_b)} - 1} \tag{2}$$

where T_b is the equivalent blackbody temperature. The solid radiation angle Ω_b represents the geometric angle at which the external light source illuminates the system. To account for the environmental effects, an ambient light contribution I_{T_s,Ω_s} is introduced, satisfying $\Omega_s + \Omega_b = 4\pi$. The angular frequency of the emitted photon is determined by the energy gap between the transition states, $\omega = \Delta E/\hbar$. Finally, the photoreaction-diffusion dynamics of the ternary system can be written as

$$\begin{aligned}
\frac{\partial\phi_A}{\partial t} &= \sum_{i=A}\sum_{j=B,C,M} D_{ij}\nabla\left[\phi_i\phi_j\nabla\mu_{ij}\right] + \sum_{x=b,s} B_A I_{T_x,\Omega_x}(\omega_A)\left[\phi_M \exp\left(\frac{E_M - E_A}{k_B T_x}\right) - \phi_A\right] \\
\frac{\partial\phi_B}{\partial t} &= \sum_{i=B}\sum_{j=A,C,M} D_{ij}\nabla\left[\phi_i\phi_j\nabla\mu_{ij}\right] + \sum_{x=b,s} B_B I_{T_x,\Omega_x}(\omega_B)\left[\phi_M \exp\left(\frac{E_M - E_B}{k_B T_x}\right) - \phi_B\right], \\
\frac{\partial\phi_C}{\partial t} &= \sum_{i=C}\sum_{j=A,B,M} D_{ij}\nabla\left[\phi_i\phi_j\nabla\mu_{ij}\right]
\end{aligned} \tag{3}$$

where D_{ij} is the diffusion coefficient between components i and j, and $\mu_{ij} = \mu_i - \mu_j$ is the chemical potential difference. $E_i = \mu_i - k_B T_s \ln\phi_i$, and $B_{A/B}$ are the Einstein coefficients for the A/B ⇌ M light processes. These equations have forms similar to the dynamic equations for catalysis-induced phase separation[27] but the interactions between components are also considered. We parameterize the incident spectrum using the equivalent blackbody temperature T_b(b = A,B). The numerical computation of Eq. (3) confirms that global illumination can

drive the ternary mixture into robust periodic states, extending the binary framework to multicomponent photopatterning.

In the following, we aim to determine the critical conditions for the onset and disappearance of periodic structures, as well as the relationship between their characteristic length scale and incident light intensity.

Linear Stability Analysis

Linear stability analysis determines the critical conditions for the onset of periodic structures. The perturbations are expanded in Fourier space as follows:

$$\delta\phi_i(\mathbf{r},t) = \sum_k \delta\phi_i(\mathbf{k},t)\, e^{i\mathbf{k}\cdot\mathbf{r}} \tag{4}$$

Although the model contains four species, A, B, C and the photoexcited intermediate M, the incompressibility constraint allows one variable to be eliminated. Here, we use $\phi_M = 1 - \phi_A - \phi_B - \phi_C$, so that the linear stability problem is formulated in terms of the three independent perturbations $\delta\phi_A$, $\delta\phi_B$, $\delta\phi_C$, consistent with the numerical implementation. The linearized equations then decouple for each wave vector $\mathbf{k}$, giving

$$\frac{\partial}{\partial t}\begin{pmatrix} \delta\phi_A(\mathbf{k},t) \\ \delta\phi_B(\mathbf{k},t) \\ \delta\phi_C(\mathbf{k},t) \end{pmatrix} = \Gamma(\mathbf{k}) \begin{pmatrix} \delta\phi_A(\mathbf{k},t) \\ \delta\phi_B(\mathbf{k},t) \\ \delta\phi_C(\mathbf{k},t) \end{pmatrix} \tag{5}$$

where $\Gamma(\mathbf{k})$ is the growth-rate matrix determined by the Jacobian of the reaction kinetics and diffusion operators evaluated at the steady state. The explicit form of the linearized operator is written as a 3×3 matrix as follows:

$$\Gamma(\mathbf{k}) = \begin{pmatrix} a_{11}(\mathbf{k}) & a_{12}(\mathbf{k}) & a_{13}(\mathbf{k}) \\ a_{21}(\mathbf{k}) & a_{22}(\mathbf{k}) & a_{23}(\mathbf{k}) \\ a_{31}(\mathbf{k}) & a_{32}(\mathbf{k}) & a_{33}(\mathbf{k}) \end{pmatrix} \tag{6}$$

where each matrix element is defined by the linear response of the evolution operator with respect to the composition fields, $a_{ij} \equiv \delta\mathcal{R}_i/\delta\phi_j$, $i,j \in \{A, B, C\}$. Here, $\mathcal{R}_i$ denotes the right-hand side of the evolution equation for component i, $\partial\phi_i/\partial t = \mathcal{R}_i$ and the explicit expressions of all a_{ij} are provided in the electronic supplementary information (ESI).

The linear stability of the homogeneous steady state is determined by the three eigenvalues λ_1, λ_2 and λ_3 of $\Gamma(\mathbf{k})$. Rather than assigning the instability to a prescribed eigenvalue branch, we characterize the stability using the maximal real part, $\lambda_+(\mathbf{k}) = \max_i \mathrm{Re}[\lambda_i(\mathbf{k})]$. The homogeneous state is linearly stable if $\lambda_+(\mathbf{k}) < 0$ for all nonzero $\mathbf{k}$, whereas finite-wavelength instability occurs when $\lambda_+(\mathbf{k}) > 0$ for at least one finite $\mathbf{k}$. Further analysis shows that $\lambda_+ = 0$ holds identically at $\mathbf{k} = 0$. Consequently, a Turing bifurcation can occur only if the slope of λ_+ at the origin is negative, that is, $\partial\lambda_+/\partial k < 0$ at $\mathbf{k} = 0$, and $\lambda_+(\mathbf{k}) > 0$ for some $\mathbf{k}$.

Thus, the critical light intensity for the emergence of periodic structures is identified as T_0, at which $\partial\lambda_+/\partial\mathbf{k} = 0$ at $\mathbf{k} = 0$. In addition, the upper critical point at which periodic structures disappear, T_c, is obtained by first imposing the marginal-stability condition that $\lambda_+(\mathbf{k}) \le 0$ for all $\mathbf{k} \neq 0$. The detailed derivation is provided below and in the ESI. For the globally illuminated case, our linear stability analysis is restricted to perturbations around the steady homogeneous state; the stability of strongly nonstationary, far-from-steady morphologies is beyond the scope of the present analysis. The critical intensity T_c predicted by the linear stability analysis is in quantitative agreement with those extracted from the numerical simulations.

Pattern Formation and Scaling Relations

The numerical simulation results for the three-component system are shown in Fig. 1(a). Self-organized structures are clearly observed. With increasing equivalent blackbody temperature, periodic structures persist and their characteristic length scale remains continuously tunable. To sustain dissipative structures, B molecules generated within A-rich regions must be transported over distances comparable to the domain size toward the B-rich regions. Increasing illumination enhances B production and increases the dissipation demand at interfaces; both effects favor smaller domains, thereby reducing the characteristic length scale. The characteristic length scale can be extracted from the simulated concentration fields using Fourier-space scattering analysis. Additional parameter effects and statistical analysis methods are provided in the ESI. In all cases, the characteristic structural length scale satisfies $\xi \sim \exp\left[\frac{s\Delta E}{k_B T_b}\right]$. From the slope extracted in Fig. 1(a), the parameter $s = 0.275$ in the labyrinthine phase was found to be in agreement with previous studies on ternary phase-separating systems coupled with ideal reactions.[28,29] Because component C is not photoactive but can still be microphase-separated, the effective slope s extracted in the multicomponent system is smaller than that in the binary case. Lattice-based discretization is employed to better capture the diffusive coupling between components, as discussed in the **DISCUSSION** section.

Entropy Production and Nonequilibrium Phase Transitions

Fig. 1(b) shows that the entropy production rate exhibits a distinct jump during a nonequilibrium phase transition. A similar phenomenon, accompanied by a phase transition and a discontinuous change in entropy production, was reported by Tomé *et al.*[30] For photo-driven systems, the system is maintained far from equilibrium, and the total entropy production arises primarily from two distinct contributions: entropy production associated with diffusive transport and that generated during photo-induced interconversion reactions, $\dot{S} = \dot{S}_D + \dot{S}_v$. In a previous study,[18] the entropy production for binary systems was systematically derived for both contributions. In our system, the entropy production associated with diffusion inside the reactive and nonreactive regions can be expressed separately as:

$$\dot{S}_D = \frac{\rho_0}{T}\int d\mathbf{r} \sum_{i,j}^{A/B/C/M} D_{ij}\phi_i\phi_j \left|\nabla\mu_{ij}\right|^2 \tag{7}$$

Within the illuminated region, Bose-Einstein statistics imply that the entropy associated with a photon depends on the blackbody temperature, giving $\dot{s} = \hbar\omega/T_b$.[31] Accordingly, the total entropy change arising from photon emission and absorption can be written as:

$$\begin{aligned}\dot{S}_v = \rho_0 k_B \int d\mathbf{r} \sum\nolimits_{x\in b,s} & B_0 I_{T_x}(\omega_A)\left[\ln\phi_M - \ln\phi_A + \frac{\Delta E_{MA}}{k_B T_x}\right]\times \\ & \left(\phi_M \exp\left(\frac{\Delta E_{MA}}{k_B T_x}\right) - \phi_A\right) + B_0 I_{T_x}(\omega_B)\left[\ln\phi_M - \ln\phi_B + \frac{\Delta E_{MB}}{k_B T_x}\right]\times \\ & \left(\phi_M \exp\left(\frac{\Delta E_{MB}}{k_B T_x}\right) - \phi_B\right)\}\end{aligned} \tag{8}$$

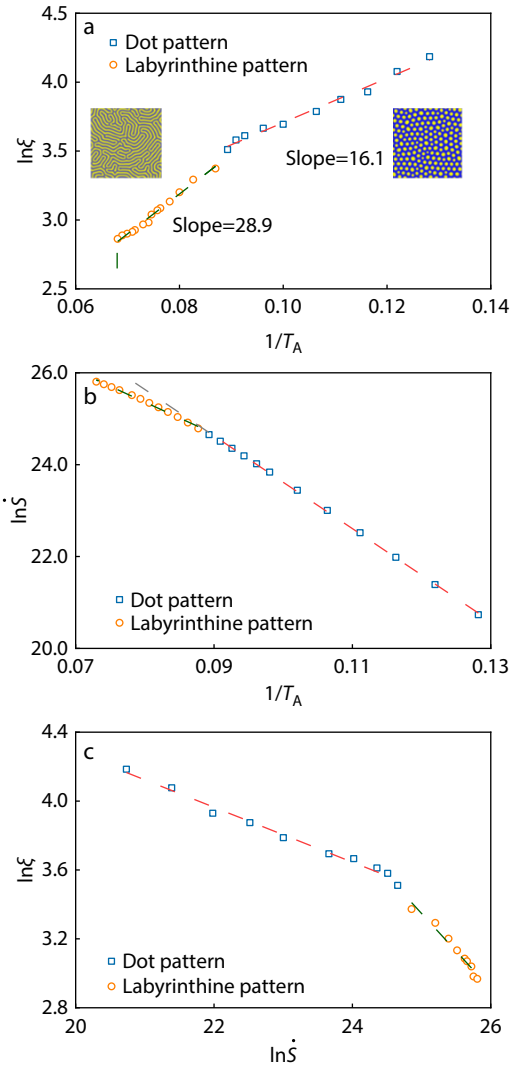

Fig. 1 (a) Relationship between the characteristic length scale and the equivalent blackbody temperature. The equivalent blackbody temperature T_A is expressed in units of T_s. The slope in the labyrinthine pattern is given by $s\Delta E_A/(k_B T_s) = 28.9$, with $s = 0.275$. The cutoff corresponds to $1/T_A = 0.068 \approx 1/14.7$, which coincides with the result of linear stability analysis. Simulations are performed on a 514×514 system under periodic boundary conditions with parameters $k_B T_s = 1$, $T_B = 15.5T_s$, $D = 0.5$, $\chi = 4.0$, $b_{A/B/C} = 1$, $B_A = B_B = 1$, $\epsilon_A = 15k_B T_s$, $\epsilon_B = 0$, $\epsilon_M = 120k_B T_s$, and $t = 5 \times 10^6\tau$. (b) Relationship between the total entropy production and the equivalent blackbody temperature. In both phases, the entropy production exhibits an approximately linear dependence on the incident light intensity. Although the two fitted lines appear visually similar, their slopes differ substantially, with slopes of approximately −68 (labyrinthine) and −100 (dot). (c) Relationship between the characteristic length scale and the total entropy production. During pattern transitions, $\dot{S}$ changes accordingly, while within each pattern regime a linear relation holds between $\ln\xi$ and $\ln\dot{S}$.

In Fig. 1(c), entropy production provides a sensitive descriptor of the nonequilibrium phase transition: when the transition occurs, $\dot{S}$ exhibits a pronounced jump, consistent with the step-like change in the characteristic length scale at the same point. Although the system displays distinct morphologies across the transition, overall linear scaling remains valid. In the labyrinthine phase, $\ln\xi$ and $\ln\dot{S}$ obey a linear relationship with slope 1/2, that is, $\dot{S} \sim \xi^2$. By contrast, the scaling exponent in the dot phase is approximately 1/6, that is, $\dot{S} \sim \xi^6$. We speculate that the emergence of the dot pattern is associated with suppressed Ostwald ripening, combined with nucleation-and-growth effects. The detailed mechanism and scaling relations between the entropy production rate and characteristic length will be discussed in our future work.

These results show that global illumination provides a controllable route to periodic structures in multicomponent nonequilibrium mixtures and may extend to more complex reaction networks.

PHASE DIAGRAM UNDER LOCAL ILLUMINATION

Model Construction

Most existing studies on photo-driven reaction-diffusion systems are restricted to globally homogeneous reaction conditions. In contrast, realistic chemical and biological systems are typically characterized by spatially localized energy input, which gives rise to confined reactive regions and, consequently, strong reaction-diffusion coupling accompanied by pronounced spatial gradients. Such heterogeneous energy injection may induce nonequilibrium ordered structures that cannot emerge under uniform global driving.[32] Localized illumination provides a minimal yet physically reasonable model for describing spatially confined energy acquisition and signal activation in living systems, thereby offering insight into how a spatially heterogeneous energy supply regulates nonequilibrium self-organization.

Based on these considerations, localized illumination is introduced into the simulation framework. Specifically, the circular region of radius r centered at the middle of the system is subjected to external illumination and is defined as the reactive domain $\mathcal{D}_r$, representing a localized energy-input region under natural conditions. Outside this domain, only weak ambient illumination I_s is present, whose corresponding photoreaction rate is negligible compared with that inside $\mathcal{D}_r$, as schematically illustrated in Fig. 2.

Considering components A and C as representative examples, the corresponding rate equations can be written separately for the regions inside and outside the reactive domain:

$$\frac{\partial \phi_A}{\partial t} = \begin{cases} \sum_{i=A}\sum_{j=B,C,M} D_{ij}\nabla\left[\phi_i\phi_j\nabla\mu_{ij}\right] & \text{in } D_r \\ + \sum_{x\in b,s} B_A I_{T_x,\Omega_x}(\omega_A)\left[\phi_M \exp\left(\frac{\Delta E_{MA}}{k_B T_x}\right) - \phi_A\right] & \\ \sum_{i=A}\sum_{j=B,C,M} D_{ij}\nabla\left[\phi_i\phi_j\nabla\mu_{ij}\right] & \text{out of } D_r \\ + B_A I_{T_s,\Omega_s}(\omega_A)\left[\phi_M \exp\left(\frac{\Delta E_{MA}}{k_B T_s}\right) - \phi_A\right] & \end{cases}$$

$$\frac{\partial \phi_C}{\partial t} = \sum_{i=C}\sum_{j=A,B,M} D_{ij}\nabla\left[\phi_i\phi_j\nabla\mu_{ij}\right] \quad (9)$$

When the photoreaction rate significantly exceeds the diffusion rate (the crossover regime, in which both processes are comparable, is beyond the scope of the present study), the pattern formation behavior induced by photo-driven reaction-diffusion coupling is clearly revealed in the phase dia-

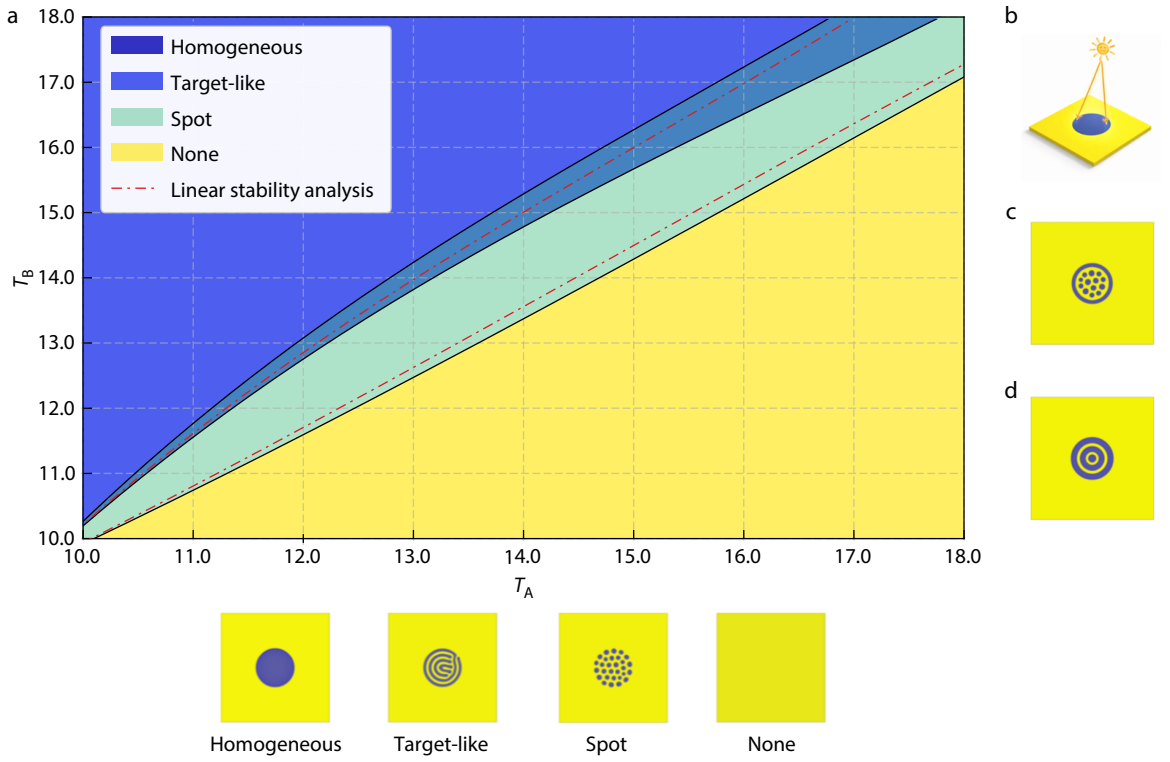

Fig. 2 (a) Phase diagram of periodic structures formed in the system under localized illumination. The simulations are performed on a 514 × 514 domain with a reaction-domain radius of $r = 96$ under periodic boundary conditions. The parameters are $k_BT_s = 1$, $D = 1$, $\chi = 4.0$, $b_{A/B/C} = 1$, $B_A = B_B = 1$, $\epsilon_{A/B} = 0$, $\epsilon_M = 120k_BT_s$, and $t = 3 \times 10^6\tau$. (b) Schematic illustration of localized illumination. (c) A cell-like structure exhibiting an intact membrane-like boundary with periodic patterns emerging at the center. (d) A strictly centrosymmetric target pattern formed at the center.

gram shown in Fig. 2(a). By varying the incident light intensities associated with components A and B, a sequence of nonequilibrium ordered structures emerges. Throughout the following discussion, the initial concentration of component A is kept sufficiently low to suppress the macroscopic phase separation. Under this condition, increasing the incident light intensity of component B progressively enhances the photo-induced conversion from B to A.

At a low photoreaction strength of component B, characterized by a small T_B, no pronounced pattern formation is observed; instead, the concentration fields exhibit only weak spatial heterogeneity arising from the non-uniform illumination. Upon increasing the incident light intensity, reaction-driven instabilities are amplified and eventually destabilize the homogeneous state, leading to the spontaneous emergence of spatially periodic structures. Under localized illumination (as demonstrated in Fig. 2b), two representative classes of nonequilibrium patterns are observed: spot patterns and target-like patterns. This classification is further supported by the corresponding Fourier-space scattering spectra. The pattern selection sequence is consistent with pattern-selection behavior. Under globally uniform illumination, in which dot patterns with relatively short characteristic wavelengths typically emerge first, as shown in Fig. 2(a).

Pattern Formation under Localized Illumination

Within the spot-pattern regime, a distinct morphology characterized by a closed boundary enclosing a stable dissipative interior structure is observed (Fig. 2c). These structures exhibit a clear separation between the boundary and interior regions and bear a qualitative resemblance to microscale cellular organization. Their formation can be attributed to the continuous increase in negative entropy input induced by illumination. As the photoreaction strength increases, the interfaces within the spot patterns sharpen and evolve into membrane-like structures, promoting the emergence of more regular and strongly periodic ordered states. Within an appropriate parameter range, the characteristic length scales of these nonequilibrium structures remain continuously tunable.

In contrast, target-like patterns frequently exhibit periodic structures that contain defects. Owing to the spatial confinement imposed by the localized illumination, periodic ordering cannot readily extend beyond the reactive domain. In this regime, diffusion-driven instabilities alone are insufficient to sustain large-scale ordered structures outside the illuminated region, and the resulting patterns can be regarded as spatially truncated lamellar-like phases.

In addition to target-like morphologies, localized target patterns are occasionally observed (Fig. 2d), indicating that reaction kinetics continue to play a decisive role in pattern selection. When the incident light intensity of either component A or B is too low, photo-induced reactions are insufficient to destabilize the homogeneous state, and the system remains in a disordered or weakly inhomogeneous regime.

The cell-like structures shown in Figs. 2(c) and 2(d) should be emphasized, as these results suggest a possible mechanism for membrane formation. In this simple model, B acts as

https://doi.org/10.1007/s10118-026-3753-z

an amphiphilic component and accumulates at the boundaries of the structures, separating A and C. Furthermore, the B-rich boundaries spontaneously enclose the photoreactive regions (active regions), resembling the function of membranes in cells.[33]

Derivation of the Theoretical Phase Diagram

The theoretical phase boundaries obtained from the linear stability analysis are shown to be in reasonable quantitative agreement with those extracted from the numerical simulations (red curves in Fig. 2a). For a localized system, phase separation and photoreaction are mainly confined to the illuminated region. The theoretical curves in Fig. 2(a) should be interpreted as semi-quantitative local stability estimates for the illuminated interior region, rather than as exact finite-domain stability boundaries of the full non-uniform localized system. Therefore, we perform linear stability analysis as a local interior stability analysis within the reactive domain. When the illumination radius r is significantly larger than the characteristic pattern wavelength, the interior of the reactive domain can be approximated as macroscopically homogeneous to the leading order. The steady state used in the linear stability analysis is then determined by the local photoreaction balance, such that the gradient and diffusive terms are not explicitly included in the steady-state calculation. This approximation is appropriate in the present parameter regime, in which the photoreaction rate is much larger than the diffusive relaxation rate. Therefore, boundary effects are weakened in the interior, although they may still influence the outer shell, defect arrangement, and confined morphology. In addition, owing to the sharply localized concentration profiles, which are primarily determined by χ and b, the interfacial width is much smaller than the pattern length scale.

Under these assumptions, the temporal evolution of component ϕ_Z(Z = A,B) can be written as

$$\frac{\partial \phi_Z}{\partial t} = \sum_{x\in\{b,s\}} B_0 I_{T_x,\Omega_x}(\omega_Z)\left[\phi_M \exp\left(\frac{\Delta E_{MZ}}{k_B T_x}\right) - \phi_Z\right] = 0 \qquad (10)$$

where $\Delta E_{MZ} = E_M - E_Z$ and $\omega_Z = \Delta E_{MZ}/\hbar$. In the parameter regime considered here, the contribution of background radiation is negligibly small. Although the factor $\exp(\Delta E_{MZ}/(k_B T_s))$ can be large for the background temperature T_s, the corresponding spectral intensity $I_{T_s,\Omega_s}(\omega_Z)$ is vanishingly small. Therefore, the contribution of background radiation to the stimulated reaction term is neglected, and the reaction is dominated by externally imposed illumination. We then define the reaction rates as $k \approx k_0\Omega_b/4\pi e^{-\Delta E/(k_B T_b)}$, where $k_0 = B_0\hbar(\Delta E/(\hbar c))^3/\pi^2$. With these definitions, the local photochemical reaction term can be written as $R_Z = (k_{0Z} + k_Z)\phi_M - k_Z\phi_Z$. By using the four-species incompressibility constraint $\phi_A + \phi_B + \phi_C + \phi_M = 1$ and $\phi_C = \phi_C^0$ in the equations, the local detailed-balance relations give

$$\phi_M^0 = \frac{1-\phi_C^0}{1+K_A+K_B}, \phi_A^0 = \frac{K_A(1-\phi_C^0)}{1+K_A+K_B}, \phi_B^0 = \frac{K_B(1-\phi_C^0)}{1+K_A+K_B} \qquad (11)$$

where $K_A = (k_{0A} + k_A)/k_A$ and $K_B = (k_{0B} + k_B)/k_B$.

$$\Gamma_0 = \begin{pmatrix} -(k_{0A}+2k_A) & -(k_{0A}+k_A) & -(k_{0A}+k_A) \\ -(k_{0B}+k_B) & -(k_{0B}+2k_B) & -(k_{0B}+k_B) \\ 0 & 0 & 0 \end{pmatrix} \qquad (12)$$

Based on the linear stability framework introduced above, we define $q \equiv \mathbf{k}^2$ is defined as follows: The eigenvalues $\lambda_i(q)$ of $\Gamma(q)$ determine the stability of the homogeneous state and the maximal growth rate is defined as $\lambda_+(q) = \max_i \mathrm{Re}[\lambda_i(q)]$. The lower critical intensity T_0 is determined from the long-wavelength behavior of $\lambda_+(q)$ (orange curve in Fig. 3). At $q = 0$, all diffusion terms vanish, and $\Gamma(q)$ is reduced to the reaction matrix.

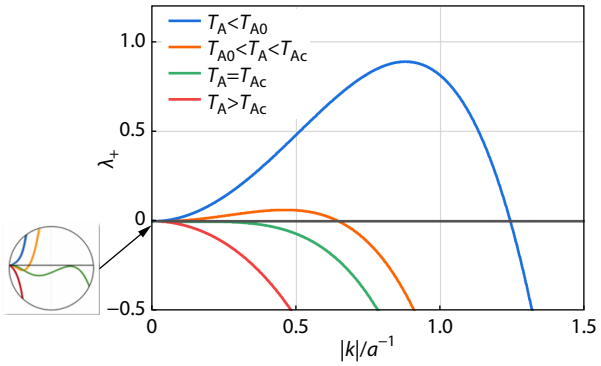

Fig. 3 Results of the linear stability analysis showing the growth rate λ_+ as a function of the wave number for different effective light intensities, with $T_B = 15.0T_s$. For $T_A = 13.8T_s$, the system undergoes macroscopic phase separation (blue curve). At $T_A = 15.3T_s$, a finite-wave-number instability develops, giving rise to periodic structures (orange curve), with $T_{A0} = 14.0T_s$. The critical light intensity at which the periodic instability vanishes is $T_{Ac} = 15.5T_s$ (green curve). For $T_A = 16.0T_s$, all growth rates remain negative, and no pattern formation is observed (red curve).

Although component C does not participate directly in the photoreaction, it enters the reaction Jacobian through the incompressibility constraint. Therefore, a perturbation in ϕ_C changes ϕ_M and modifies the local photoreaction rates. Consequently, the reaction matrix at $q = 0$ generally contains nonzero elements in the third column. $\Gamma(0)$ has one zero eigenvalue λ_1 and two strictly negative eigenvalues λ_2 and λ_3. We expand the growth matrix near $q = 0$ as follows: $\Gamma(q) = \Gamma(0) + q\Gamma^{(1)} + O(q^2)$, where $\Gamma^{(1)} = \mathrm{d}\Gamma/\mathrm{d}q|_{q=0}$ and $O(q^2)$ denotes the terms of the second and higher orders in q. The coefficient $\Gamma^{(1)}$ is determined by the first-order correction to this neutral branch. The eigenvalue branch emerging from the zero eigenvalue has the small-q expansion $\lambda_1(q) = q\sigma + O(q^2)$, where $\sigma = a_{33}^{(1)} - \phi_A^0/(1-\phi_C^0)a_{31}^{(1)} - \phi_B^0/(1-\phi_C^0)a_{32}^{(1)}$. For a diffusion operator with equal diffusivities $D_{ij} = D$, the long-wavelength neutral branch is unstable to the first order in q when

$$\frac{2\chi_{AC}\phi_C^0(1-\phi_C^0)(k_{0A}+k_A)k_B}{k_{0A}k_B + k_A k_{0B} + 3k_A k_B} < 1 \qquad (13)$$

The upper critical intensity T_c which corresponds to the disappearance of finite-wavelength periodic structures, is obtained from the finite-q neutral stability condition (green curve in Fig. 3). For $\Gamma(q)$, the characteristic polynomial is $\lambda^3 - T(q)\lambda^2 + S(q)\lambda - P(q) = 0$ where $T(q) = \mathrm{tr}\Gamma(q)$, $S(q)$ is the sum of the second-order principal minors, and $P = \det\Gamma(q)$. A neutral finite-wavelength mode satisfies $\lambda(q_c) = 0$ and therefore $P(q_c) = 0$. $P(q)$ contains a factor q^2 Therefore, $P(q) = q\mathcal{Q}(q)$ with $\mathcal{Q}(q) = P_1 + P_2 q + P_3 q^2 + P_4 q^3 + P_5 q^4 + P_6 q^5$. Nonzero neutral modes are obtained from

$P_1 + P_2q + P_3q^2 + P_4q^3 + P_5q^4 + P_6q^5, q > 0$. The physically relevant q_c is selected as $\mathcal{Q}(q_c) = 0, \mathcal{Q}'(q_c) = 0, q_c > 0$ together with the branch-consistency conditions $T(q_c) < 0, S(q_c) > 0$. The corresponding critical wavenumber is $|\mathbf{k_c}| = \sqrt{q_c}$. The explicit form of $\Gamma(q)$ the coefficients $P_1 - P_6$ and the detailed derivation of the lower and upper critical conditions are provided in the ESI.

Overall, linear stability analysis captures the main parameter window in which locally illuminated systems support finite-wavelength periodic structures. The smaller instability window predicted by the theoretical phase diagram is due to the nonlinear and spatially inhomogeneous processes present in the simulations, including boundary-induced concentration gradients and finite-domain effects, which are not fully included in the homogeneous linear stability analysis.

Nevertheless, under appropriate conditions, localized energy input is sufficient to induce distinct characteristic structures that are otherwise inaccessible in homogeneous environments. Experimental studies have consistently shown that photochemical reactions can drive phase behavior and generate unique microstructures under nonequilibrium conditions,[19,34–36] lending additional support to the mechanisms identified here. Although a direct connection with biological systems remains to be established, these findings suggest that a spatially heterogeneous energy supply may play a constructive role in promoting structural diversity in active and living matter. In this sense, our study extends the applicability of reaction-diffusion models to nonequilibrium scenarios relevant to prebiotic chemistry, origin of life, and biological organization far from equilibrium.

DISCUSSION

Nonnegativity of Entropy Production

Nonnegativity constitutes a fundamental theoretical requirement for reaction-diffusion models, as it ensures that the proposed dynamics provide a physically realistic description of nonequilibrium processes. Eqs. (7) and (8) can both be cast into the form $\left(e^X - e^Y\right)(X - Y)$, which is strictly non-negative. Therefore, the entropy production rates associated with both diffusion and photoreaction processes are non-negative. Fig. 4 shows that the entropy production obtained from the numerical simulations under both global and localized illumination conditions remains non-negative and is dominated by contributions arising from the emergence and stabilization of periodic structures, which are primarily generated by photo-induced reactions.

Comparison between Two Diffusion Terms

For multicomponent incompressible mixtures, diffusion can be represented by different mobility approximations, provided that the resulting mobility matrix preserves the free-energy dissipation. A commonly used choice is the constant-mobility form $D_{ij}\nabla^2\mu_{ij}$, which is analogous to the standard Model-B-type approximation. In this work, we consider a composition-dependent pairwise mobility, $D_{ij}\nabla\left[\phi_i\phi_j\,\nabla\mu_{ij}\right]$. This form is motivated by the Onsager picture of local exchange between species and is well suited to Flory-Huggins-type phase-separating mixtures.[27] The two diffusion operators should be regarded as two thermodynamically admissible but physically different approximations. However, systematic comparisons have been limited. In practice, the influence of the mobility choice is often weak at the level of the initial linear instability but becomes evident during nonlinear evolution and in the final steady patterns.

The distinction becomes clear in numerical simulations, where species that do not participate directly in the photoreactions may still be coupled through diffusion and thus influence the post-instability evolution. This behavior is illustrated in Fig. 5, where non-coupled and coupled diffusion yield qualitatively different steady states, and two-phase coexistence is strongly suppressed in the coupled case.

The origin of this discrepancy can be traced to the distribution of dissipation during droplet evolution. For the constant-mobility form $D_{ij}\nabla^2\mu_{ij}$, dissipation associated with chemical potential fluctuations occurs throughout both the bulk and interfacial regions, leading to bulk-mediated coupling between domains.[37] After phase separation, a substantial fraction of the free-energy decrease is consumed by the bulk relaxation modes, while the coarsening and droplet interactions continue toward the steady state. Under these condi-

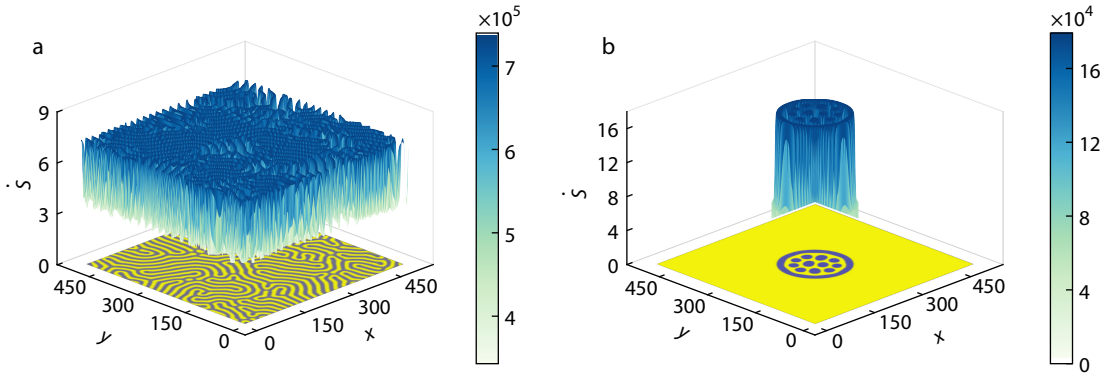

Fig. 4 Spatial distribution of the entropy production rate. The total entropy production rate of the system is given by $\dot{S} = \dot{S}_D + \dot{S}_v$. In the bottom-plane morphology map of component A, blue denotes A-rich regions, where higher entropy production is also observed. (a) Spatial distribution of the entropy production rate under homogeneous illumination. (b) Spatial distribution of the entropy production rate under localized illumination. Under realistic conditions, the presence of ambient light leads to a small but finite entropy production rate in the non-reactive region; this contribution is treated as background noise and is therefore not shown.

https://doi.org/10.1007/s10118-026-3753-z

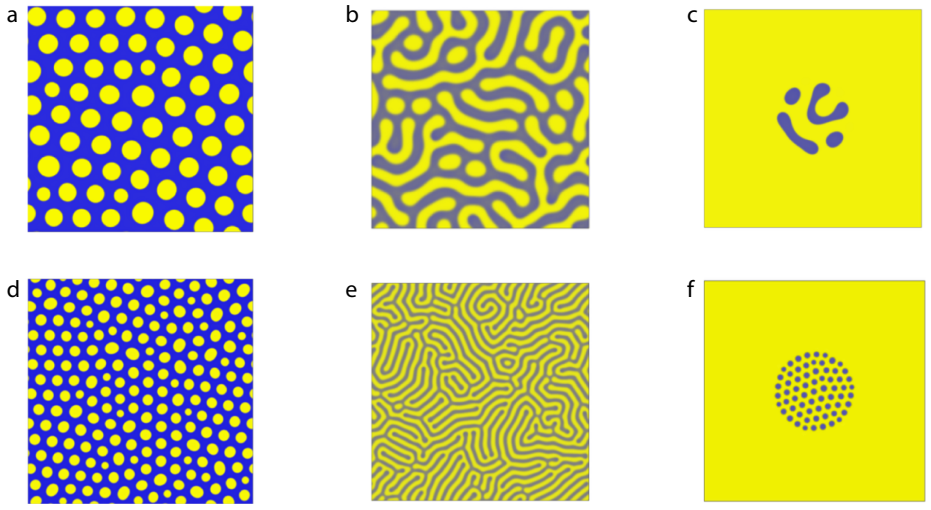

Fig. 5 Morphological comparison for two diffusion formulations. Panels (a–c) show results obtained with the constant-mobility (non-coupled) diffusion operator, whereas panels (d–f) correspond to the multiplicative (coupled) diffusion operator. For (a, d), $T_A = 11.0T_s$, $T_B = 15.5T_s$, $D = 0.5$, $\epsilon_A = 15k_BT_s$, and $t = 5 \times 10^6\tau$; for (b, e), $T_A = 13.7T_s$, $T_B = 15.5T_s$, $D = 0.5$, $\epsilon_A = 15k_BT_s$, and $t = 5 \times 10^6\tau$; for (c, f), $T_A = 11.8T_s$, $T_B = 13.5T_s$, $D = 0.5$, $\epsilon_A = 15k_BT_s$, and $t = 5 \times 10^6\tau$. All other parameters are identical for the two diffusion operators.

tions, dot-like domains tend to grow and gradually connect, producing labyrinthine patterns in space (Figs. 5a and 5b).

By contrast, the multiplicative form $D_{ij}\nabla\left[\phi_i\phi_j\nabla\mu_{ij}\right]$ introduces a degenerate, state-dependent mobility that vanishes in pure-phase regions, thereby confining dissipation primarily to narrow interfacial zones. As a result, the non-intersecting domains interact only weakly and remain pinned as long-lived droplet states.[38] Once the external negative entropy input is sufficiently strong to promote extended interfacial connectivity, the ensuing coarsening becomes strongly biased and drives the system toward labyrinthine-pattern-dominated behavior (Figs. 5d and 5e).

A closely analogous trend is observed under localized illumination (Figs. 5c and 5f): the coupled diffusion operator is required to reproduce the dot microstructures, whereas the constant-mobility form mainly yields coarse, bulk-separated domains with larger characteristic length scales. Moreover, the constant-mobility operator may become numerically ill-conditioned as $\phi_i \to 0$, because the ideal-mixing term implies $\ln(\phi_i) \to -\infty$. In practice, mild regularization is often necessary to avoid spurious transport.

Taken together, these results show that diffusion operators may lead to different pattern selections at long times in multicomponent reaction-diffusion systems. These phenomenological consequences motivate the use of thermodynamically consistent composition-dependent diffusion operators when modeling multicomponent reaction-diffusion systems in the nonlinear regime. The finite-difference discretization used for the diffusion terms is provided in the ESI. A mathematically rigorous comparison of the two diffusion formulations will be pursued in future studies.

Application in Polymer Systems

The present photoreaction-diffusion model can be viewed as a coarse-grained framework for light-regulated morphology control in polymeric soft matter. Several generic control parameters that are broadly relevant to photoresponsive polymer systems are identified. In photoresponsive polymer blends, photopolymerization-induced phase separation, photo-crosslinking systems, and supramolecular block copolymer assemblies, irradiation can modify the effective composition, mobility, or transient molecular states. These light-induced changes are often coupled with phase separation and interfacial transport, leading to reaction-diffusion-controlled morphology selection.[19,25,39,40]

Beyond these experimental motivations, an increasing number of light-responsive polymers and supramolecular systems can be interpreted within the minimal framework proposed herein. In this picture, light does not merely trigger a chemical event but also continuously regulates the local composition and activity of the system. The resulting imbalance between photoreaction, diffusion, and phase separation provides a general route to nonequilibrium self-assembly.

The value of the proposed model for polymer systems lies in its design principles. Under global illumination, the characteristic length scale follows a light-controlled scaling relation, suggesting that the domain spacing can be tuned by adjusting the photon energy, effective light intensity, or molecular energy parameters. Under localized illumination, spatially confined energy inputs produce dot-like, target-like, and cell-like dissipative structures, which are relevant to polymer films, hydrogels, photocurable resins, and soft materials patterned by masks or focused beams. Therefore, the multicomponent photoreaction-diffusion model may serve as a theoretical template for understanding and designing light-driven self-assembly of polymer chains under nonequilibrium conditions.

CONCLUSIONS

In this study, we extend photoreaction-driven reaction-diffusion coupling models from conventional binary systems to a multicomponent framework. Using a ternary system as a minimal model, numerical simulations combined with linear stabili-

ty analysis systematically demonstrate that illumination can drive the system into periodically ordered nonequilibrium states. Moreover, the characteristic length scale of the resulting structures can be continuously tuned by adjusting the incident light intensity or molecular internal energy parameters, satisfying $\ln\xi \sim \frac{s\Delta E}{k_B T_b}$. Motivated by the fact that energy input in realistic chemical and biological systems is often spatially heterogeneous, we introduced localized illumination to model energy injection within confined reactive regions. Under localized illumination, a theoretical phase diagram for pattern formation was constructed based on numerical simulations and linear stability analysis. Multiple classes of spatially ordered structures were identified, including dot and target-like patterns. Within specific parameter regimes, confined dissipative states with well-defined boundaries and internally ordered structures were observed. These morphologies exhibit qualitative similarities with the microscale cellular structures. These findings extend the applicability of reaction-diffusion models in the context of the origin of life and provide a physical picture of how localized energy inputs may facilitate the emergence of spatial order in nonequilibrium systems.

In addition, the entropy production was examined in both globally and locally illuminated models. By explicitly evaluating the nonnegativity of entropy production, we verified that the system dynamics satisfy the fundamental constraints of nonequilibrium thermodynamics, thereby ensuring the physical reliability of the proposed framework. Finally, we compared pattern-formation behaviors arising from different diffusion coupling forms within the reaction-diffusion model. This comparison shows that the choice of diffusion operator can qualitatively influence the resulting steady-state patterns, even when the reaction kinetics and linear stability conditions are identical.

Conflict of Interests

The authors declare no interest conflict.

Electronic Supplementary Information

Electronic supplementary information (ESI) is available free of charge in the online version of this article at http://doi.org/10.1007/s10118-026-3753-z.

Data Availability Statement

The data supporting the findings of this study are available within the article and ESI. Additional data are available from the corresponding author upon reasonable request.

ACKNOWLEDGMENTS

This work was financially supported by the National Natural Science Foundation of China (Nos. 22373022 and 52394272), the National Key Research and Development Program of China (No. 2023YFA0915300), and the Shanghai Science and Technology Innovation Action Plan (No. 24JD1400700). The authors thank Prof. Shigeyuki Komura for helpful discussions.

REFERENCES

1 Witzany, G. Crucial steps to life: from chemical reactions to code using agents. *Biosystems* **2016**, *140*, 49–57.
2 Goldbeter, A. Dissipative structures in biological systems: bistability, oscillations, spatial patterns and waves. *Philos. Trans. R. Soc. A* **2018**, *376*, 20170376.
3 Zwicker, D.; Seyboldt, R.; Weber, C. A.; Hyman, A. A.; Jülicher, F. Growth and division of active droplets provides a model for protocells. *Nat. Phys.* **2017**, *13*, 408–413.
4 De Domenico, M. Decoding the architecture of living systems. *Rep. Prog. Phys.* **2026**, *89*, 014601.
5 Zampetaki, A. V.; Liebchen, B.; Ivlev, A. V.; Löwen, H. Collective self-optimization of communicating active particles. *Proc. Natl. Acad. Sci. U.S.A.* **2021**, *118*, e2111142118.
6 Volpert, V.; Petrovskii, S. Reaction-diffusion waves in biology: new trends, recent developments. *Phys. Life Rev.* **2025**, *52*, 1–20.
7 Kondo, S.; Asai, R. A reaction-diffusion wave on the skin of the marine angelfish pomacanthus. *Nature* **1995**, *376*, 765–768.
8 Sick, S.; Reinker, S.; Timmer, J.; Schlake, T. WNT and Dkk determine hair follicle spacing through a reaction-diffusion mechanism. *Science* **2006**, *314*, 1447–1450.
9 Ait Mahiout, L.; Bessonov, N.; Kazmierczak, B.; Sadaka, G.; Volpert, V. Infection spreading in cell culture as a reaction-diffusion wave. *ESAIM: Math. Model. Numer. Anal.* **2022**, *56*, 791–814.
10 El Hajj, W.; El Khatib, N.; Volpert, V. Inflammation propagation modeled as a reaction–diffusion wave. *Math. Biosci.* **2023**, *365*, 109074.
11 Potts, J. R.; Petrovskii, S. V. Fortune favours the brave: movement responses shape demographic dynamics in strongly competing populations. *J. Theor. Biol.* **2017**, *420*, 190–199.
12 Glotzer, S. C.; Di Marzio, E. A.; Muthukumar, M. Reaction-controlled morphology of phase-separating mixtures. *Phys. Rev. Lett.* **1995**, *74*, 2034.
13 Carati, D.; Lefever, R. Chemical freezing of phase separation in immiscible binary mixtures. *Phys. Rev. E* **1997**, *56*, 3127.
14 Longo, T. J.; Shumovskyi, N. A.; Asadov, S. M.; Buldryev, S. V.; Anisimov, M. A. Structure factor of a phase separating binary mixture with natural and forceful interconversion of species. *J. Non-Cryst. Solids: X* **2022**, *13*, 100082.
15 Aslyamov, T.; Avanzini, F.; Fodor, É.; Esposito, M. Nonideal reaction-diffusion systems: multiple routes to instability. *Phys. Rev. Lett.* **2023**, *131*, 138301.
16 Manz, N.; Davydov, V. A.; Zykov, V. S.; Müller, S. C. Excitation fronts in a spatially modulated light-sensitive Belousov-Zhabotinsky system. *Phys. Rev. E* **2002**, *66*, 036207.
17 Hildebrand, M.; Skødt, H.; Showalter, K. Spatial symmetry breaking in the Belousov-Zhabotinsky reaction with light-induced remote communication. *Phys. Rev. Lett.* **2001**, *87*, 088303.
18 Li, C.; Li, J.; Zhang, H.; Yang, Y. A systematic study on immiscible binary systems undergoing thermal/photo reversible chemical reactions. *Phys. Chem. Chem. Phys.* **2023**, *25*, 1642–1648.
19 Yue, B.; Jia, X.; Baryshnikov, G. V.; Jin, X.; Feng, X.; Lu, Y.; Luo, M.; Zhang, M.; Shen, S.; Ågren, H.; et al. Photoexcitation-based supramolecular access to full-scale phase-diagram structures through in situ phase-volume ratio phototuning. *Angew. Chem. Int. Ed.* **2022**, *61*, e202209777.
20 Krause, A. L.; Klika, V.; Woolley, T. E.; Gaffney, E. A. From one pattern into another: analysis of Turing patterns in heterogeneous domains via WKBJ. *J. R. Soc. Interface* **2020**, *17*, 20190621.
21 Van Gorder, R. A. Pattern formation from spatially heterogeneous

Graphical Abstract

From Global to Localized Illumination: Tunable Photo-induced Patterns in a Ternary Reaction-diffusion System

Zhuo-Hang Cai, Chang-Hao Li, and Jian-Feng Li

Fudan University; Zhejiang University; Xiangshan Hospital of Wenzhou Medical University

Photo-induced multicomponent reaction-diffusion systems provide a valuable theoretical framework for exploring nonequilibrium self-organization under external energy input. Illumination can induce tunable nonequilibrium periodic structures whose characteristic length scale satisfies $\ln\xi \sim \frac{s\Delta E}{k_B T_b}$. Furthermore, distinct spatial morphologies can also be observed under local illumination and a theoretical phase diagram for pattern formation is constructed.

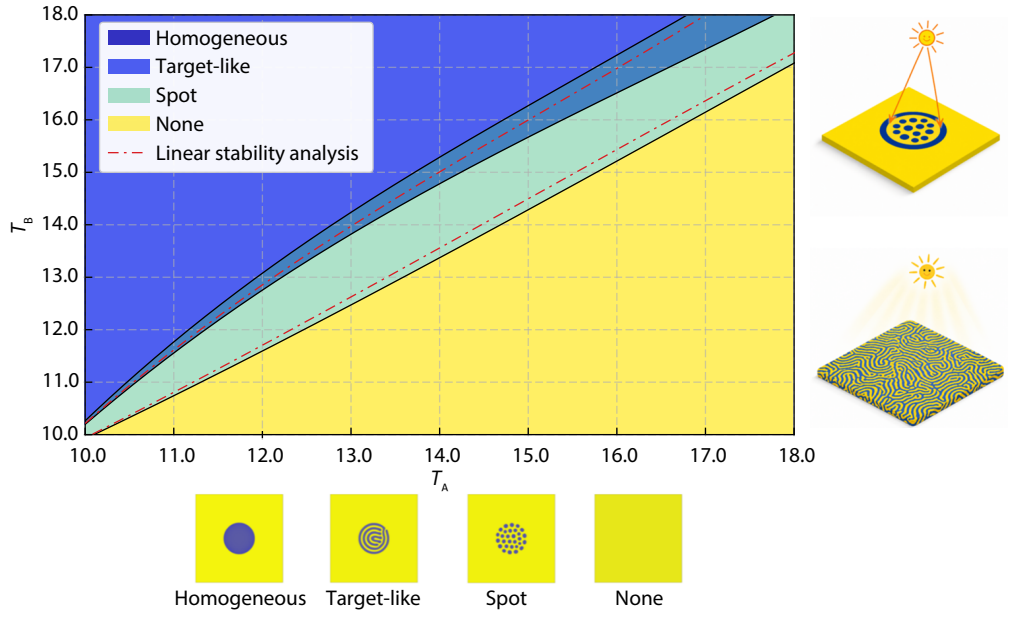

Chinese J. Polym. Sci., 2026 *https://doi.org/10.1007/s10118-026-3753-z*

reaction–diffusion systems. *Philos. Trans. R. Soc. A* **2021**, *379*, 20210001.

22 Penocchio, E.; Rao, R.; Esposito, M. Nonequilibrium thermodynamics of light-induced reactions. *J. Chem. Phys.* **2021**, *155*, 114101.

23 Tran-Cong, Q.; Ohta, T.; Urakawa, O. Soft-mode suppression in the phase separation of binary polymer mixtures driven by a reversible chemical reaction. *Phys. Rev. E* **1997**, *56*, R59–R62.

24 Tran-Cong, Q.; Harada, A.; Kataoka, K.; Ohta, T.; Urakawa, O. Positive feedback driven by concentration fluctuations in asymmetrically photo-cross-linked polymer mixtures. *Phys. Rev. E* **1997**, *55*, R6340–R6343.

25 Zhang, Y.; Liang, X.; Yang, C.; Tang, Y.; Yan, Q. Light-fueled non-photoisomerized dissipative self-assembly system through transient radical-radical interactions. *Angew. Chem. Int. Ed.* **2025**, *64*, e202512915.

26 Landau, L. D.; Lifshitz, E. M. *Statistical Physics*; Elsevier, **2013**; Vol. 5. p. 187.

27 Cotton, M. W.; Golestanian, R.; Agudo-Canalejo, J. Catalysis-induced phase separation and autoregulation of enzymatic activity. *Phys. Rev. Lett.* **2022**, *129*, 158101.

28 Liu, B.; Tong, C.; Yang, Y. The kinetics and phase patterns in a ternary mixture coupled with chemical reaction of A + B ⇌ C. *J. Phys. Chem. B* **2001**, *105*, 10091–10100.

29 Tong, C.; Zhang, H.; Yang, Y. Phase separation dynamics and reaction kinetics of ternary mixture coupled with interfacial chemical reaction. *J. Phys. Chem. B* **2002**, *106*, 7869–7877.

30 Tomé, T.; de Oliveira, M. J. Entropy production in nonequilibrium systems at stationary states. *Phys. Rev. Lett.* **2012**, *108*, 020601.

31 Li, C.; Li, J.; Yang, Y. First-principle derivation of single-photon entropy and Maxwell–Jüttner velocity distribution. *Entropy* **2022**, *24*, 1609.

32 Mahato, R. R.; Adikessavane, N.; Ettikkan, N. K.; Maiti, S. A chemoenzymatic reaction-diffusion system with local inhibition and distal activation. *Nat. Commun.* **2025**, *16*, 9885.

33 Eisenmann, I.; L'homme, A.; Lahlou, A.; Bujaldon, S.; Le Saux, T.; Bailleul, B.; Desprat, N.; Jeanneret, R. Light-induced phase separation with finite wavelength selection in photophobic microalgae. *Phys. Rev. Lett.* **2025**, *135*, 148401.

34 Torra, J.; Campelo, F.; Garcia-Parajo, M. F. Tensing flipper:

photosensitized manipulation of membrane tension, lipid phase separation, and raft protein sorting in biological membranes. *J. Am. Chem. Soc.* **2024**, *146*, 24114−24124.
35 Li, J.; Li, T.; Ma, X.; Su, Z.; Yin, J.; Jiang, X. Light-induced programmable 2D ordered patterns based on a hyperbranched poly(ether amine)(HPEA)-functionalized graphene film. *ACS Appl. Mater. Interfaces* **2020**, *13*, 1704−1713.
36 Zheng, J.; Chen, J.; Jin, Y.; Wen, Y.; Mu, Y.; Wu, C.; Wang, Y.; Tong, P.; Li, Z.; Hou, X.; Tang, J. Photochromism from wavelength-selective colloidal phase segregation. *Nature* **2023**, *617*, 499−506.
37 Barrett, J. W.; Blowey, J. F.; Garcke, H. Finite element approximation of the Cahn–Hilliard equation with degenerate mobility. *SIAM J. Numer. Anal.* **1999**, *37*, 286−318.
38 Barrett, J. W.; Blowey, J. F.; Garcke, H. On fully practical finite element approximations of degenerate Cahn-Hilliard systems. *ESAIM: Math. Model. Numer. Anal.* **2001**, *35*, 713−748.
39 Müller, M. Z.; Bernero, M.; Xie, C.; Qiu, W.; Oggianu, E.; Rabut, L.; Michaels, T. C. T.; Style, R. W.; Müller, R.; Qin, X. H. Cell-guiding microporous hydrogels by photopolymerization-induced phase separation. *Nat. Commun.* **2025**, *16*, 4923.
40 Biria, S.; Hosein, I. D. Control of morphology in polymer blends through light self-trapping: an in situ study of structure evolution, reaction kinetics, and phase separation. *Macromolecules* **2017**, *50*, 3617−3626.

https://doi.org/10.1007/s10118-026-3753-z